

Analysis of Asymmetric Aircraft Aerodynamics Due to an Experimental Wing Glove

Fletcher Hartshorn¹

TYBRIN Corporation, NASA Dryden Flight Research Center, Edwards AFB, CA 93523

Aerodynamic computational fluid dynamics analysis of a wing glove attached to one wing of a business jet is presented and discussed. A wing glove placed on only one wing will produce asymmetric aerodynamic effects that will result in overall changes in the forces and moments acting on the aircraft. These changes, referred to as deltas, need to be determined and quantified to ensure that the wing glove does not have a significant effect on the aircraft flight characteristics. TRANAIR (Calmar Research Corporation, Cato, New York), a non-linear full potential solver, and Star-CCM+ (CD-adapco, Melville, New York), a finite volume full Reynolds-averaged Navier-Stokes computational fluid dynamics solver, are used to analyze a full aircraft with and without the glove at a variety of flight conditions, aircraft configurations, and angles of attack and sideslip. Changes in the aircraft lift, drag, and side force along with roll, pitch, and yaw are presented. Span lift and moment distributions are also presented for a more detailed look at the effects of the glove on the aircraft. Aerodynamic flow phenomena due to the addition of the glove are discussed. Results show that the glove produces only small changes in the aerodynamic forces and moments acting on the aircraft, most of which are insignificant.

Nomenclature

AGPS	= aerodynamic grid and paneling system
Alpha	= aircraft angle of attack, deg
Beta	= aircraft angle of sideslip, deg
CD	= drag force coefficient (non-dimensionalized by wing planform area)
CFD	= computational fluid dynamics
C_L	= lift force coefficient (non-dimensionalized by wing planform area)
C_Y	= side force coefficient (non-dimensionalized by wing planform area)
C_l	= rolling moment coefficient (non-dimensionalized by wing planform area, wing span)
C_m	= pitching moment coefficient (Non-dimensionalized by wing planform area, mean aerodynamic chord)
C_n	= yawing moment coefficient (Non-dimensionalized by wing planform area, wing span)
D	= global grid cell size
DPW	= drag prediction workshop
FDS	= flux differencing scheme
H	= altitude, ft
LE	= leading edge
M	= Mach number
MAC	= mean aerodynamic chord
NASA	= National Aeronautics and Space Administration
NEPP	= NASA engine performance program
NLF	= natural laminar flow
OEI	= one engine inoperable
RANS	= Reynolds-averaged Navier-Stokes
SST	= shear-stress-transport
TRL	= technology readiness level
V	= velocity, ft/s

¹ Aerospace Engineer, Aerodynamics and Propulsion Branch, P.O. Box 273, M/S 4840B, AIAA Member.

V2	=	takeoff safety speed, ft/s
y+	=	non-dimensional wall height
1D	=	one-dimensional
2D	=	two-dimensional
3D	=	three-dimensional
Δ	=	delta
ρ	=	density, slugs/ft ³

Subscripts

∞	=	freestream conditions
X	=	X direction (stream-wise, positive downstream)
Y	=	Y direction (span-wise, positive out the right wing)
Z	=	Z direction (vertical, positive up)

I. Introduction

National Aeronautics and Space Administration (NASA) Dryden Flight Research Center does a significant amount of work testing new technologies to benefit aviation. One current project at NASA Dryden uses a business jet as a test bed for flight testing experiments and raising their technology readiness levels (TRL). One of the current major experiments is a high Reynolds number, natural laminar flow (NLF) airfoil that will be flight-tested in the form of a wing glove. The wing glove will be placed on the left wing of the aircraft and will cover approximately one quarter of the aircraft half-span. The glove will most likely produce asymmetric aerodynamic effects on the aircraft because it is placed on only the left wing, and has different aerodynamic characteristics than the business jet. These effects need to be analyzed and quantified in order to determine if the wing glove will present problems in the flight of the aircraft.

Many different concerns are raised with having a glove attached to one wing of the aircraft. For example, structural problems may arise if the aerodynamic loads are very different in magnitude or direction on the glove than the clean wing. The main concern of this paper, however, is how the asymmetric loads of the glove affect the overall handling and controllability of the aircraft. This is quantified by finding the amount of control surface deflection required in order to mitigate the added aerodynamic asymmetries from the glove. The results will be used to assess the aerodynamics of the wing glove on the overall aircraft aerodynamics.

TRANAIR¹ (Calmar Research Corporation, Cato, New York), a non-linear full potential code directly coupled with a boundary layer model, will be used to perform most of the analysis on the entire aircraft. The Aerodynamic Grid Paneling System (AGPS)² is used to create the surface grids for all of the TRANAIR computations. The DPW-3 DLR-F6 wing/body no fairing, no engine geometry is used to perform grid independence studies in AGPS and TRANAIR because of the availability of test data and the standard configuration of the geometry. Star-CCM+³ (CD-adapco, Melville, New York), a finite volume full Reynolds-averaged Navier-Stokes (RANS) computational fluid dynamics (CFD) code, will be used for low-speed, high-flap deflection, high beta, and one engine inoperable (OEI) flight conditions. The description of the codes, grid setup, and solver setup are described in great detail so that one might be able to replicate the results presented in this paper for future studies. All of the analysis is performed on the business jet with and without the glove attached.

II. Code Validation

Before any CFD code can accurately be applied to an engineering problem, background work such as validation studies and grid independence studies need to be performed. These studies will help show that TRANAIR and Star-CCM+ are very robust and accurate within the limits of their capabilities.

A. Code Descriptions

TRANAIR is used for predicting subsonic, transonic and supersonic flow about arbitrary configurations. TRANAIR is a three-dimensional (3D) finite element, non-linear full potential flow solver directly coupled with an integral boundary layer model. The boundary layer model employed is two-dimensional (2D) with added wing sweep and taper corrections that allow it to be applied to wing-like and axisymmetric body surfaces.⁴ The boundary layer is computed along sets of longitudinal strings of points, called strips.⁵ TRANAIR has the ability to specify regions with different total pressure and temperatures for different flow properties such as engine plumes. A discrete Green's function for the Prandtl-Glauert equation is used at the far-field boundaries of the domain, which operates under the assumption that flow is linear outside of the domain.⁶ The grid used is based off of a fully structured

paneled surface. TRANAIR has the ability to use a linearly abutted set of networks where the code interpolates between the abutting nodes. The unstructured solution adaptive Cartesian volume grid is automatically generated and superimposed on the boundary defined by the surface grid.⁷ The solution adaptive grid is refined where the error estimates from the velocity gradients are high. This allows TRANAIR to efficiently capture highly non-linear effects such as shocks and pressure peaks, while coarsening the grid where the flow is linear.⁵ The solution is obtained on a sequence of locally refined grids given cell count and size limits from the user.

Star-CCM+, which is developed by CD-adapco, is a finite volume solver for steady state and time-accurate flow computations. Star-CCM+ has the ability to use both pressure-based and density-based solvers that are compatible with RANS, large eddy simulation, and detached eddy simulation models. Star-CCM+ is developed to solve structured and unstructured meshes, but can be used to create unstructured tetrahedral, polyhedral, or trimmed hexahedral grids. The polyhedral grid is created using a special dualization scheme and is based on an underlying tetrahedral mesh. CD-adapco claims that a standard polyhedral mesh has approximately five times fewer cells than a tetrahedral mesh, given the same starting surface.⁸ The savings in cell count while retaining similar solution accuracy is a major benefit of using a polyhedral mesh for complex geometries.

B. Code Validation and Grid Independence

TRANAIR has been validated numerous times for aircraft cruise configurations, and is considered a very robust and accurate code. A specific validation study was performed by Edward N. Tinoco using the DLR-F6 geometry.⁹ Star-CCM+ is also a validated RANS code, one example of which is CD-adapco's entry into the 3rd AIAA Drag Prediction Workshop (DPW).¹⁰ The best practices and methods established by CD-adapco and the AIAA are used in generating the grids for this paper.

TRANAIR is used more in this paper, therefore, more validation and grid studies were performed with TRANAIR than Star-CCM+. Figure 1 shows the final surface paneling of the DLR-F6 based on the results of the grid independence studies.

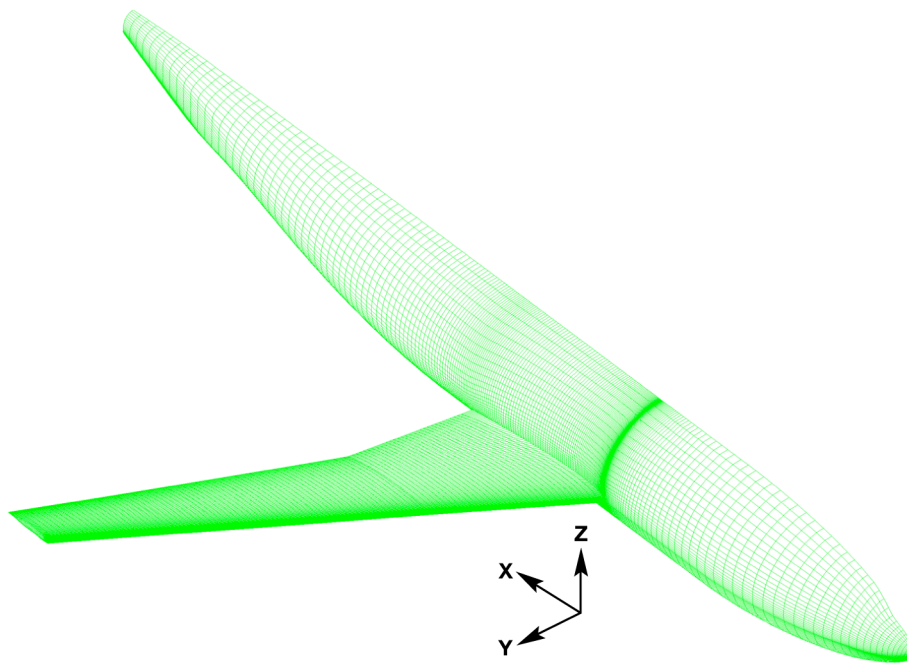


Figure 1. Surface paneling on the DLR-F6 geometry.

The grid independence studies are performed to quantify the effect of the surface grid size, volume grid size, and domain size on the solution. These results are very useful in selecting the gridding parameters for the full business jet aircraft geometry used in this paper. The spanwise surface resolution is varied from 25 to 150 sections. As the number of span sections increases above 75, there is only a 0.1% difference in solution lift and drag forces. The grid points along the chord are also varied from 101 to 401. The difference in solution forces between the grids with higher than 201 points is only 0.5%. It seems that the solution is slightly more sensitive to chord resolution than

span surface resolution. For the purposes of evaluating the overall controllability of the aircraft, 0.1% and 0.5% are acceptable accuracies. From the results of this study, a conservative number of span points (105) and chord points (201) are chosen to be used for the DLR-F6 and the main business jet surface grid.

Volume grid independence is investigated by varying the initial grid size, total final cell count, and the minimum and maximum cell sizes allowable near the wing. The initial global grid size in the streamwise direction (DX) is varied from 32 units to 128 units. Coarsening the grid from 32 units to 64 units changes the final solution by only 0.1%. Further coarsening from 64 units to 128 units changes the solution by 0.6%. For the most accurate solution, the aspect ratio of the boxes should be close to one (i.e. $DX/DY, DY/DZ, et\ cetera = 1$). The accuracy on which far field effects are resolved improves with decreasing cell size.⁵ An error of 0.1% is sufficient for the purposes of the present study and so a grid size of 64 units is used for the initial business jet volume grid.

Intuitively, decreasing the minimum cell size around specific regions of interest such as leading edges and shocks should result in more accurate solutions, but this is not always the case. For the DLR-F6, as the minimum cell size decreases, and the total cell count remains the same, the solution diverges slightly from the comparison results.¹⁰ When the minimum cell size is decreased, more cells are clustered around the suction peak, leaving fewer cells to capture the oblique shocks effectively. Decreasing the max cell size has a similar effect. One way to mitigate the decrease in accuracy is to increase the overall cell count, so that all of the flow phenomena can be modeled sufficiently. However, cell count is directly related to solution time; so for example, doubling the cell count will roughly double the solution time. In the following full business jet analysis, a variety of total cell counts are analyzed with similar maximum and minimum sizes to determine grid independence with the fastest solution time.

The size of the computational domain is an important factor in the accuracy of the solution. In TRANAIR, the computational domain needs only to include the configuration surfaces, significant flow regions, and a small buffer zone of two cells for numerical reasons.⁵ The size of the domain is not usually very large in subsonic computations. The baseline size chosen in each direction away from the configuration surfaces is listed in Table 1. Increasing the distance of the aft domain to two full body lengths changes the solution by 0.02%. Likewise, varying the size in all other directions has insignificant effects on the solution. All of the results from the grid studies on the DLR-F6 will be applied to the creation of the business jet grid.

Table 1. Size of the baseline TRANAIR computational domain.

Domain direction	Length from aircraft
Front	Half body length
Aft	Full body length
Above	Full body length
Below	Full body length
Right	One chord length

III. Business Jet Analysis

The aircraft geometry and generated grids are described in detail in order to obtain a better understanding of the problem and how it is approached. The solver settings and analysis matrix are presented as well to provide a complete picture of the analysis and allow for repeatability by future persons.

A. Geometry

The business jet is a low-wing configuration, with aft body mounted engines, and a T-tail. The glove, seen in Fig. 2, is placed on the left wing starting at approximately the 45% half span location and extends six feet outboard.

The blue piece is the main test section, the red are the fairings that help smooth the cross flow over the wing to provide a clean test section surface, and the black part is the blending region. The glove test section has an inboard fairing that is 3.2 ft in span and an outboard fairing 2.5 ft in span. The glove blends back into the 60% chord location of the wing with a smooth tangency and curvature controlled blend. The glove geometry is offset from the wing with 2 in of clearance, and protrudes from the leading edge of the wing by 2.3 ft.

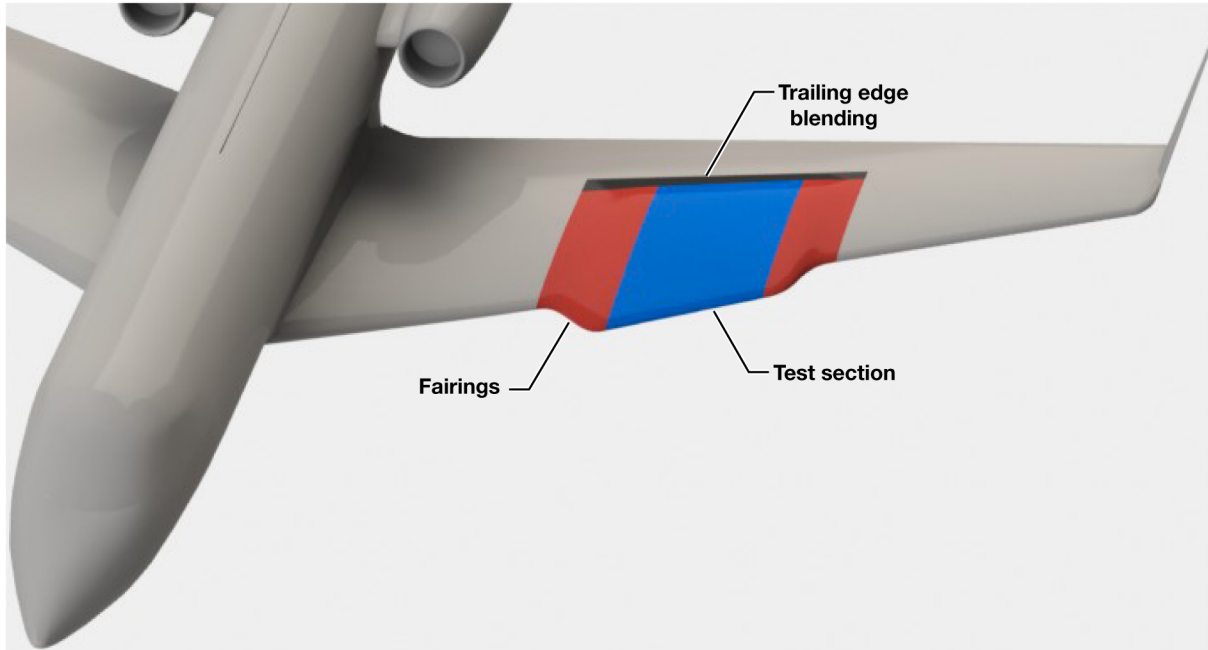


Figure 2. Glove mounted on the left wing. Blue-test section; Red-fairings; and Black-TE blending.

B. Grid Topology

TRANAIR and Star-CCM+ are different types of codes and therefore the gridding style of each varies significantly. TRANAIR uses a fully structured surface grid with a solution adaptive Cartesian volume grid. Star-CCM+ uses a fully unstructured polyhedral grid with prism layers to model the near-wall flow.

1. TRANAIR

There are two TRANAIR surface grids created for the analysis: a full aircraft configuration without the glove, and the full aircraft with the glove on the left wing. The full aircraft grid with the glove is shown in Fig. 3; the networks are in various colors to better visualize the individual grids. The surface paneling of the business jet that is used for the analysis is fully structured with a combination of point matching and linear abutments between the networks. Figure 4, shows the grid at the pylon/body intersection. The networks on an aircraft section such as the fuselage are linearly abutted in order to obtain the best grid in the most efficient manner. Point-to-point matching is used to ensure accurate discretization of the original geometry where different aircraft sections intersect, such as wing/body or nacelle/pylon.

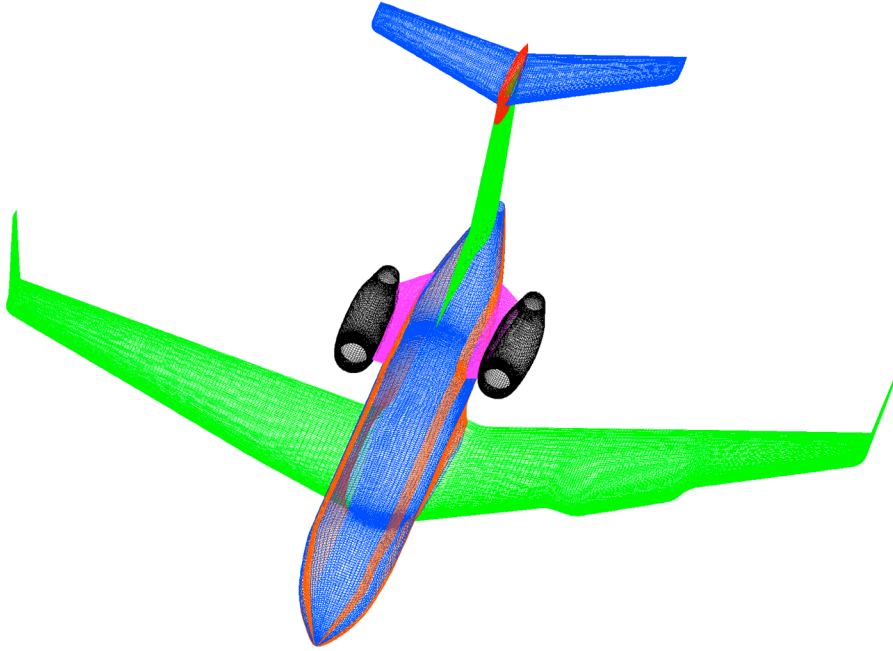


Figure 3. Surface paneling of the business jet with no glove.

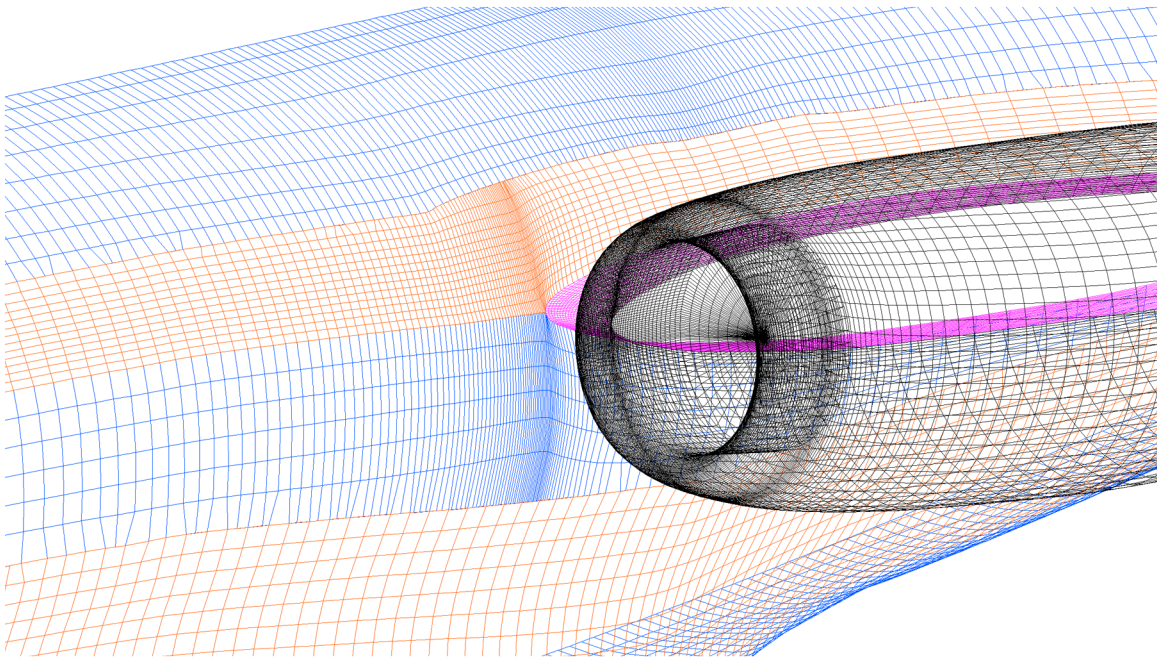


Figure 4. Surface paneling of the business jet pylon/body intersection.

TRANAIR is a full potential code; therefore, trailing edge wakes need to be modeled using surface grids to carry the viscosity and vorticity properties downstream. Figure 5 shows an example of the usage of the different types of wakes.

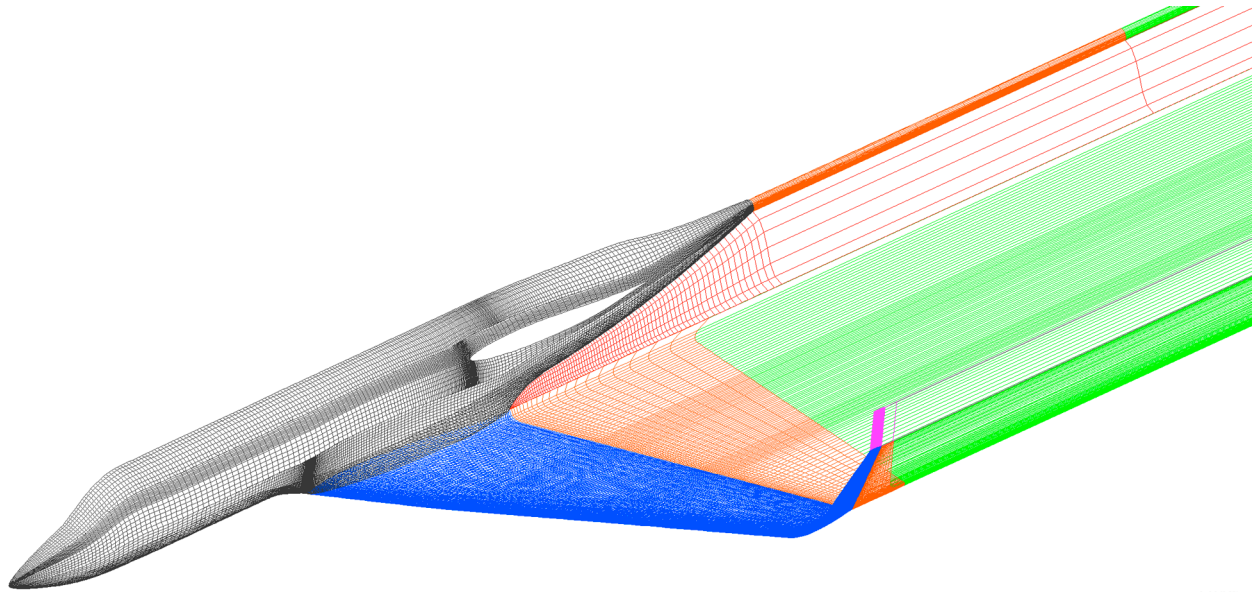


Figure 5. An example of wake grids on a portion of the business jet with no glove.

The wing and the body are solid viscous walls colored blue and gray respectively. There are three main classes of wakes used to model a full aircraft configuration: inviscid wakes, viscous wakes, and ‘design’ wakes. Inviscid wakes carry the doublet strength from the aircraft downstream. Viscous wakes are inviscid wakes that also permit simulation of thickness through transpiration, necessary to model the viscosity information from the boundary layer solver and are colored orange in Fig. 5. ‘Design’ wakes enforce the conditions of no pressure change boundaries, which are necessary in modeling powered plumes. The viscous wakes are modeled directly off of the trailing edge of a wing or axisymmetric body, and usually extend one chord length behind the surface. The boundary layer quantities computed at the trailing edges of the viscous wakes are essential for computing accurate profile drag. The inviscid wakes are used in a few different ways. One use is to extend them from the trailing edge of a viscous wake, and out the back of the computational domain, colored green in Fig. 5. Inviscid wakes are also used at wing tips (magenta) and to connect wakes from multiple bodies (red). A common usage of the connecting wakes is to carry over the wing wake to the side of the fuselage to which it connects.⁵ Similar methods are used on the wakes of the T-tail and pylon/engine combination.

The aircraft grid is modeled as a full configuration with no symmetry plane. Since the glove is only on one wing, the aircraft is not symmetric and needs to be modeled with both the left and right sides. Even though the clean aircraft is symmetric, the full aircraft was gridded in order to maintain the most similarities between the grids with and without the glove. Using a full aircraft doubles the cell count needed on the surface and in the volume, which roughly doubles the computational time from 1.2 to 2.4 hr. 2.4 hr is still fast enough that the increase in computation time is an acceptable trade off to ensure the accuracy and consistency of the solutions. The surface grids of the clean and gloved aircraft are broken down into the number of panels per aircraft segment, excluding the wakes, in Table 2. The addition of the glove in the surface paneling only results in an increase of 8,000 panels to better discretize the curvature of the glove and fairings.

Table 2. TRANAIR surface panels on business jet grid.

Aircraft section	# Surface panels without glove	# Surface panels with glove
Wing	32,000	40,000
Winglet	32,000	32,000
Nacelle	20,000	20,000
Pylon	5,000	5,000
Vertical	12,000	12,000
Vertical Cap	3,400	3,400
Horizontal	11,600	11,600
Fuselage	29,000	29,000
TOTAL	145,000	153,000

The volume grid for each solution is automatically generated by TRANAIR and adapted to refine flow features. The final volume grid is obtained by a sequence of successively refined grids that are adapted based on errors in the velocity gradients and user inputs.⁵ The final volume grid has approximately 1.7 million cells in the entire domain. The user has control of the location in the domain where the refinement takes place by specifying a box region around the desired area of refinement. Typically, these boxes are located around every feature of the aircraft including wings, body, engine, et cetera. Regions of interest such as wing leading edges (LE) usually have their own box to further refine the grid. For example, the volume grid around the leading edge of the outboard section of the wing is allowed to refine the Cartesian grid to a cell length of 0.2 in. Significant grid refinement was concentrated around the wing and the glove in order to capture the shocks at high speeds and the pressure peaks at high alphas. The volume around the vertical tail; however, is only allowed to refine to a cell length no smaller than 1.5 in because the flow around the vertical tail was not deemed critical compared to that around the wing. Regions such as wing tips, the aft part of a body, and the wing wakes are typically of little interest because the solver does not need refined volume regions around these areas.⁵

Every TRANAIR run uses the same surface grids with slightly varying volume refinement parameters, except for the ground effects analysis. A physical ground plane in TRANAIR is required in order to model ground effects. Since TRANAIR does not have the capability to have a symmetry condition about the XY plane if there is not symmetry about the XZ plane, the ground plane has to be modeled physically. The ground plane is created using a very large flat grid that is 35 ft below the aircraft, extends 3 body lengths forward and aft of the aircraft, and two span lengths on each side. Because the ground plane is fixed to be horizontal in space, the solver angle of attack has to be set at zero. Therefore, instead of specifying a change in input flow direction, the physical aircraft grid is rotated up to the appropriate alpha. When the aircraft is rotated, the wake grids need to be modified as well. The wake grids are rotated along with the aircraft, so they extend back from the aircraft, parallel to the centerline. The wake planes have to be turned parallel to the ground near the ground plane so that they will not intersect each other.

The lessons learned from the grid independence study on the DLR-F6 aircraft are used in determining the surface size, volume grid size, and domain size of the business jet aircraft. An additional grid independence study was performed using volume grid sizes of one million to two million cells. A grid size above 1.5 million cells does not show significant changes in the solution; hence, grid independence is achieved.

2. Star-CCM+

Similar to the TRANAIR grids, there are two Star-CCM+ grids for the analysis. The aircraft is modeled with flaps deployed at 20° in order to evaluate the effect that added circulation from the flaps may have on the flow over the glove. A fully unstructured triangular surface grid with curvature and proximity refinement to discretize the geometry is generated using Star-CCM+. The wing, glove, and flap are further refined to help better capture the flow gradients in the solution. Special attention is paid to the glove leading edge because it has a small radius. Fine details such as the vertical tail strake and a small slot near the wing/body trailing edge junction are captured in this model. The volume region is constructed of unstructured polyhedral cells with prismatic elements to help refine the boundary layer region. To preserve cell count, wall functions are used to calculate the properties of the boundary layer. To successfully implement wall functions, the first cell of every prism layer has an estimated non-dimensional wall height (y^+) value of 100. This puts the first cell nicely in the log-law region of the boundary layer where wall functions are designed to work.⁸ Since wall functions are used, there are only 16 prism layers on every surface of the

aircraft. The prism cells are grown from the surface with a constant stretching ratio. The number of cells and the total height of the prismatic cells are chosen for two reasons: to keep the stretching ratio below 1.4, and to ensure that the volume change between the last prismatic element and the first polyhedral cell is close to zero. This level of detail is necessary in most all CFD codes, because keeping the volume change to a minimum from cell to cell is important in improving cell quality and hence, solution quality. A full aircraft model with no symmetry plane is used because the glove is placed on only one wing. The surface mesh contains 3.8 million triangular cells, and the volume contains a total of 26 million polyhedral and prismatic cells. The cell count may seem fairly coarse for a full aircraft with no symmetry plane, but a polyhedral mesh is created from an underlying tetrahedral mesh that CD-adapco claims is typically five times its cell count.⁸ Figure 6 shows the glove and wing grids, where the wing and flap wakes are refined in order to help capture the circulation and viscous effects.

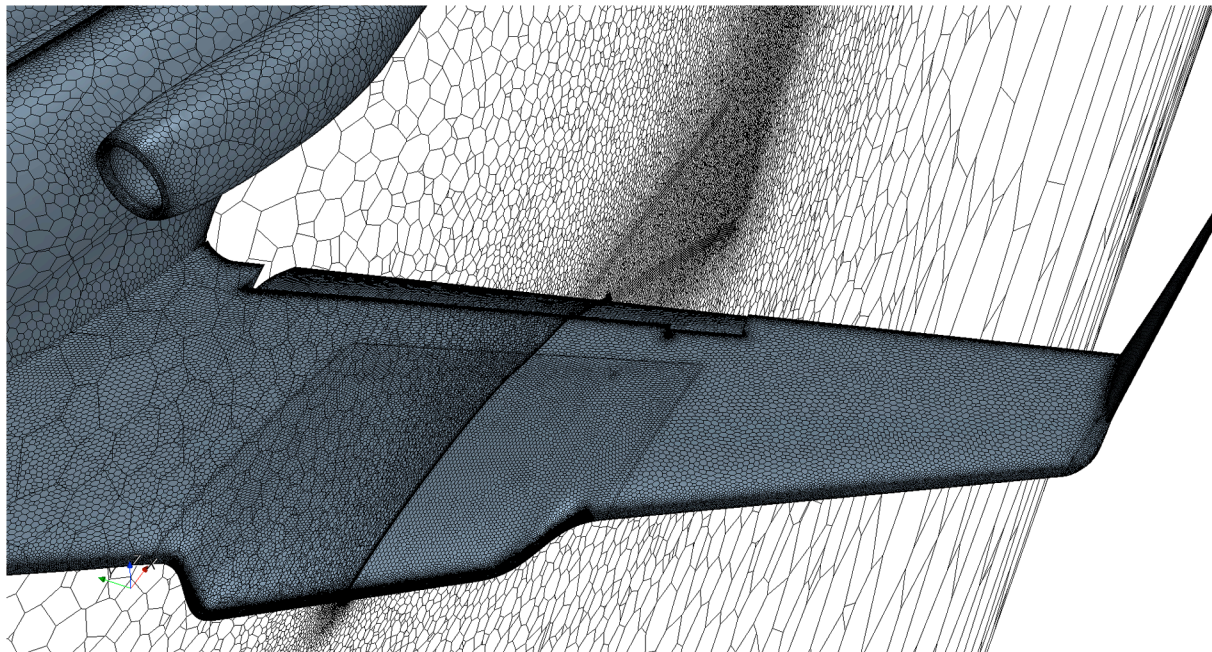


Figure 6. Unstructured polyhedral grid of the business jet with the glove.

The computational domain was placed 40 aircraft lengths behind, 20 lengths in front, 20 above, 20 below, and 20 aircraft lengths on each side to ensure no numerical contamination on the aircraft from the far field boundaries.

C. Flight Test Matrix

To determine if the glove has any detrimental effects on the aerodynamics and controllability of the aircraft, seven main flight conditions were chosen to analyze the aerodynamic characteristics of the glove:

- 1) Mach (M_∞) 0.75, Altitude (H) 45k ft
- 2) M_∞ 0.75, H 40k ft
- 3) M_∞ 0.7, H 25k ft
- 4) M_∞ 0.85, H 25k ft
- 5) M_∞ 0.26, H 0 ft
- 6) M_∞ 0.26, H 35 ft, Ground Effects
- 7) M_∞ 0.22, H 100 ft, 20° Flaps, One Engine Inoperable (OEI).

The first three flight conditions are common cruise points at which a business jet would fly and close to the proposed glove flight test conditions. The fourth flight condition is near the highest Mach and dynamic pressure limits of the aircraft, even though there is not a plan to fly there. The fifth flight condition is representative of a low speed landing and approach configuration. The sixth flight point is the same as five, but a ground plane was modeled to determine the ground effect interactions with the glove. The last flight condition is a takeoff configuration at the takeoff safety speed (V_2), to determine how the glove interacts with the flaps, along with very high beta and OEI conditions. Table 3 expands the matrix of flight conditions used for the analysis.

Table 3. Analysis matrix of flight conditions.

Flight condition	M_∞	H, ft	Alpha, deg	Beta, deg	CFD code
1	0.75	45 K	-0.76, 4.24 (1G trim)	0	TRANAIR
1	0.75	45 K	4.24 (1G trim)	± 5	TRANAIR
2	0.75	40 K	-0.76, 4.24 (trim)	0	TRANAIR
2	0.75	40 K	4.24 (1G trim)	± 5	TRANAIR
3	0.70	25 K	-2.7, 2.3 (1G trim), 6.0	0	TRANAIR
3	0.70	25 K	2.3 (1G trim)	± 5	TRANAIR
4	0.85	25 K	0.95, 1.45, 1.95 (1G trim)	0	TRANAIR
5	0.26	0	2.67, 7.67 (1G trim), 10.67	0	TRANAIR
5	0.26	0	7.67 (1G trim)	± 5	TRANAIR
6	0.26	35	7.67 (1G trim)	0	TRANAIR
7	0.22	100	6.75 (1G trim)	± 15	Star-CCM+

At each flight condition, multiple alphas and betas are analyzed. The alphas chosen are nominally trim, trim $+5^\circ$, and trim -5° , but some alterations are made in order to stay within the applicable limits of TRANAIR. Alphas greater than 11° at subsonic speeds, and alphas greater than 5° at transonic speeds are too large for TRANAIR to handle, mainly because of flow separation. The trim alpha is not changed with the addition of the glove so that the two configurations are more directly compared against one another. Betas of $\pm 5^\circ$ are analyzed at four of the flight conditions to see how the glove will affect the aircraft when it is experiencing sideslip. In the takeoff configuration, betas of $\pm 15^\circ$ are analyzed with OEI, such that the aircraft is always yawing into the dead engine. The takeoff configuration was chosen as a ‘worst’ case scenario by the recommendation of the test pilot. These last two test points are performed using Star-CCM+ because of the complex flow presented by the high yaw angle and the effect of the deflected flaps. At every flight condition and orientation angle, the clean aircraft (no glove), and the gloved aircraft are both analyzed.

D. Solver Settings

For both codes, the initial conditions for each analysis run are computed using the values specified in Table 3. The initial solver settings were chosen from past experience with similar geometry and flight conditions.

1. TRANAIR

Each TRANAIR solution is computed using seven sequenced grids running at least 2000 iterations each, or until they each reach convergence. Convergence is defined when the residuals drop by five orders of magnitude for each grid.⁵ The boundary layer model is employed over the wing and the fuselage with the appropriate sweep and taper corrections to model the effects of viscosity. The boundary layer ribs are modeled on every surface of the aircraft. However, the boundary layer model will sometimes have difficulty converging if it is in a region of adverse flow. The problem boundary layer rib can be removed to improve convergence, and the code will extrapolate the boundary layer data from the closest ribs.⁵ A second order mass flux biasing upwinding scheme is used which introduces less artificial viscosity than a first order solution.⁵ The size of the freestream domains are based on the sensitivity study that was performed by varying the size of the domain in Section II.B.

Engine boundary conditions are used to model the fan face, exhaust face, and plume effects. The engine conditions for each flight condition are obtained using the NASA Engine Performance Program (NEPP), a one-dimensional (1D) engine cycle analysis.¹¹ The inlet face is modeled by specifying the non-dimensional mass flow (ρV) along the upper surface normal of the network.⁵ The engine plume is modeled by specifying a separate material region from the freestream that has its own total temperature and pressure definitions. Thrust-drag bookkeeping is used to obtain the thrust corrected lift, drag, and pitching moment in an empirical fashion.⁵

2. Star-CCM+

The solutions are obtained using the compressible, steady state full RANS equations. The boundary layer was assumed to be fully turbulent everywhere and was modeled using the two-equation $k-\omega$ (Menter) Shear Stress Transport (SST) turbulence model.¹² Wall functions are implemented, and the solver uses a 2nd order implicit coupled Roe flux differencing scheme (FDS). The freestream conditions (i.e. the flight conditions) are modeled

using far-field boundary conditions. The boundaries are placed using the information from Section III.B.2. Similar to TRANAIR, the engines are modeled in order to capture the effects they have on the flow over the wing, and possibly the glove. The engine inlet is modeled with a pressure outlet boundary condition that uses the target mass flow option. This allows the solver to adjust the pressure at each iteration to yield a specified mass flow rate.⁸ The engine outlet is modeled using a mass flow inlet boundary condition. Similar to TRANAIR, the engine conditions are obtained using NEPP.

IV. Business Jet Results and Discussion

The results from the CFD analysis are presented in two ways: overall changes in aircraft forces and moments, and the local flow phenomena caused by the glove. The changes in aircraft forces and moments are quantified using deltas, (clean aircraft forces and moments minus those of the gloved aircraft) and also the control surface deflections that are required to trim out these deltas. The local flow phenomena are discussed using contour plots, spanwise force and moment distribution plots, and flow streamlines.

A. Aircraft Aerodynamic Configuration Results

The origin of the coordinate system is on the ground approximately 76.1 in below and 4 in inboard of the nose. The X-axis is positive going from front to aft, the Y-axis is positive out the right wing, and the Z-axis is positive up. The orientation of the coordinate system is the same as that seen in Fig. 1. Following the right hand rule, beta is defined as positive yawing to the left. Positive rolling moment (C_l) is defined as positive rolling into the left wing. Positive pitching moment (C_m) is nose up, and positive yawing moment (C_n) is into the left wing. Table 4 presents the differences, or deltas, in the forces and moments between the two configurations (no glove, and gloved).

Table 4. Delta forces and moments of the aircraft with and without the glove.

Flight condition	M_∞	H, ft	Alpha, deg	Beta, deg	ΔC_L	ΔC_D	ΔC_Y	ΔC_l	ΔC_m	ΔC_n
1	0.75	45 K	4.24	0	-0.0106	-0.0015	0.0017	-0.0012	-0.0037	-0.0003
1	0.75	45 K	-0.76	0	-0.0039	0.0002	0.0008	-0.0008	0.0019	-0.0002
1	0.75	45 K	4.24	5	-0.0120	0.0012	0.0024	-0.0007	-0.031	-0.0005
1	0.75	45 K	4.24	-5	-0.0081	-0.0044	0.0031	-0.0006	-0.0046	-0.0005
2	0.75	40 K	4.24	0	-0.0089	-0.0015	0.0016	-0.0010	-0.0041	-0.0003
2	0.75	40 K	-0.76	0	-0.0041	-0.0003	0.0009	-0.0008	0.0021	-0.0003
2	0.75	40 K	4.24	5	-0.0102	-0.0015	0.0011	-0.0012	-0.0036	-0.0003
2	0.75	40 K	4.24	-5	-0.0096	-0.0008	0.0002	-0.0016	-0.0042	0.0000
3	0.70	25 K	2.30	0	-0.0071	-0.0004	0.0012	-0.0011	-0.0026	-0.0003
3	0.70	25 K	-2.70	0	0.0005	-0.0021	0.0000	-0.0005	0.0053	0.0000
3	0.70	25 K	6.00	0	-0.0121	-0.0003	0.0023	-0.0016	-0.0066	-0.0006
3	0.70	25 K	2.30	5	-0.0073	-0.0004	0.0014	-0.0009	-0.0017	-0.0004
3	0.70	25 K	2.30	-5	-0.0069	-0.0004	0.0012	-0.0013	-0.0030	-0.0003
4	0.85	25 K	1.59	0	0.0059	-0.0013	0.0007	0.0034	-0.0038	0.0002
4	0.85	25 K	1.09	0	0.0023	-0.0016	0.0001	0.0020	-0.0005	0.0004
4	0.85	25 K	0.59	0	-0.0055	-0.0021	-0.0003	-0.0005	0.0051	0.0004
5	0.26	0	2.67	0	-0.0060	-0.0003	0.0011	-0.0011	-0.0027	-0.0003
5	0.26	0	7.67	0	-0.0103	-0.0009	0.0023	-0.0018	-0.0092	-0.0007
5	0.26	0	10.67	0	-0.0130	-0.0018	0.0028	-0.0020	-0.0129	-0.0009
5	0.26	0	7.67	5	-0.0110	-0.0011	0.0024	-0.0016	-0.0080	-0.0007
5	0.26	0	7.67	-5	-0.0099	-0.0009	0.0022	-0.0022	-0.0105	-0.0006
6	0.26	35	7.67	0	-0.0081	-0.0008	0.0014	-0.0020	-0.0032	-0.0001
7	0.22	100	6.75	15	-0.0112	-0.0038	-0.0019	-0.0011	-0.0056	0.0000
7	0.22	100	6.75	-15	-0.0075	-0.0085	0.0002	-0.0026	-0.0129	0.0000

The glove increases the overall lift of the aircraft except at very low alphas, and very high Mach and dynamic pressures. For the most part, the drag increases with the glove because of the interference effects of the test section fairings. The added lift on the left wing causes the aircraft to roll into the right wing. The glove also causes the

aircraft to have a negative yawing moment (to the right). One would expect the aircraft to yaw to the left since the glove on the left wing produces more drag than the clean wing. The increase in drag; however, is negligible and a roll/yaw coupling influences the flight dynamics to a greater extent. More lift is produced when the aircraft rolls into the right wing, which actually causes a slight yaw to the right moment.

At almost every flight condition, the glove causes a slight aircraft pitch up moment because the glove extends 2.3 ft in front of the wing leading edge. This extension is a new lift producer that is in front of the aircraft moment reference center, causing a pitch up moment. The exception to this trend is at low alphas below 1.6°. When the aircraft flies at a low alpha, the glove develops a fairly substantial region of negative lift near the leading edge. This addition of negative lift in front of the moment reference center causes the aircraft to have an additional pitch down moment, opposite of the trend seen at higher alphas.

At most flight conditions, the behavior of the glove follows similar trends and is fairly predictable. However, large shocks are evident on the wing upper surface at flight condition four, near maximum dynamic pressure. The glove changes the shock structure on the wing significantly, producing very non-linear flow causing the forces and moments to not follow the same trends as the other results. This phenomenon will be explained in greater detail in the next section.

Deltas of the coefficients are very useful in order to look at the overall changes in forces and moments on the aircraft. Finding the control surface deflections required to trim out the deltas of the forces and moments is used to quantify the magnitude of the effects that the glove has on the aircraft. A six degrees-of-freedom motion simulator is used to find the control surface deflections in Table 5, with the deltas calculated from the TRANAIR and Star-CCM+ results. The control surface deflections are found independently of each other with no coupling considerations. Aileron is used for roll control, elevator for pitch control, and rudder for yaw control.

Table 5. Control surface deflections required to trim out the deltas in the forces and moment due to the glove.

Flight condition	M_∞	H, ft	Alpha, deg	Beta, deg	ΔC_l Aileron, deg	ΔC_m Elevator, deg	C_n Rudder, deg
1	0.75	45 K	4.24	0	1.0	0.2	0.2
1	0.75	45 K	-0.76	0	0.6	-0.1	0.2
1	0.75	45 K	4.24	5	0.5	0.2	0.4
1	0.75	45 K	4.24	-5	0.5	0.3	0.4
2	0.75	40 K	4.24	0	0.8	0.3	0.2
2	0.75	40 K	-0.76	0	0.6	-0.1	0.2
2	0.75	40 K	4.24	5	0.9	0.2	0.2
2	0.75	40 K	4.24	-5	1.2	0.3	0.0
3	0.70	25 K	2.30	0	0.9	0.2	0.2
3	0.70	25 K	-2.70	0	0.4	-0.4	0.0
3	0.70	25 K	6.00	0	1.3	0.5	0.5
3	0.70	25 K	2.3	5	0.7	0.1	0.3
3	0.70	25 K	2.30	-5	1.1	0.2	0.2
4	0.85	25 K	1.59	0	-2.9	0.4	-0.2
4	0.85	25 K	1.09	0	-1.7	0.1	-0.3
4	0.85	25 K	0.59	0	0.4	-0.6	-0.3
5	0.26	0	2.67	0	0.9	0.1	0.3
5	0.26	0	7.67	0	1.4	0.5	0.6
5	0.26	0	10.67	0	1.6	0.7	0.8
5	0.26	0	7.67	5	1.2	0.4	0.6
5	0.26	0	7.67	-5	1.8	0.6	0.5
6	0.26	35	7.67	0	1.5	0.2	0.1
7	0.22	100	6.75	15	0.8	0.3	0.0
7	0.22	100	6.75	-15	1.9	0.7	0.0

The results show that only small aileron input is required to trim out the added rolling moment caused by the glove. Of the flight conditions analyzed, the maximum aileron deflection required is 2.9° deflected down on the left wing and up on the right. This would be needed for the maximum Mach and dynamic pressure flight condition. This aileron deflection is well within the margin of the aircraft's deflection capability in one direction, which leaves room for controllability of the aircraft. Only a small amount of elevator is required at all of the flight conditions. The change in yawing moment is the least significant, requiring up to only 0.8° of rudder deflection, which is well within the limits of the aircraft. Modeling the aircraft in ground effects did not produce any adverse results. At takeoff speeds, the circulation from the flaps did not seem to have a large effect on the flow over the glove. Also, having the aircraft in a very high beta and OEI condition did not alter the effects the glove had on the aircraft aerodynamics. The overall lift for the baseline aircraft at this flight condition is roughly equal to the maximum weight of the aircraft, and the drag is lower than the maximum thrust produced by one engine. The addition of the glove increases the lift causing an increase in the lift to weight ratio, and the increase in drag still puts the overall drag well below the maximum thrust of one engine. Overall, the added moments seen by the aircraft due to the glove are fairly insignificant and can be easily trimmed out.

B. Local Flow Properties of the Glove and Regions of Interest

Since there were no major issues resulting from the changes in forces and moments on the aircraft, the paper will now focus on the local flow effects around the glove. Mach contours on the upper surface of the clean and gloved wings are compared for flight condition two at $M_\infty 0.75$, H 40,000 ft, and 4.24° alpha in Fig. 7.

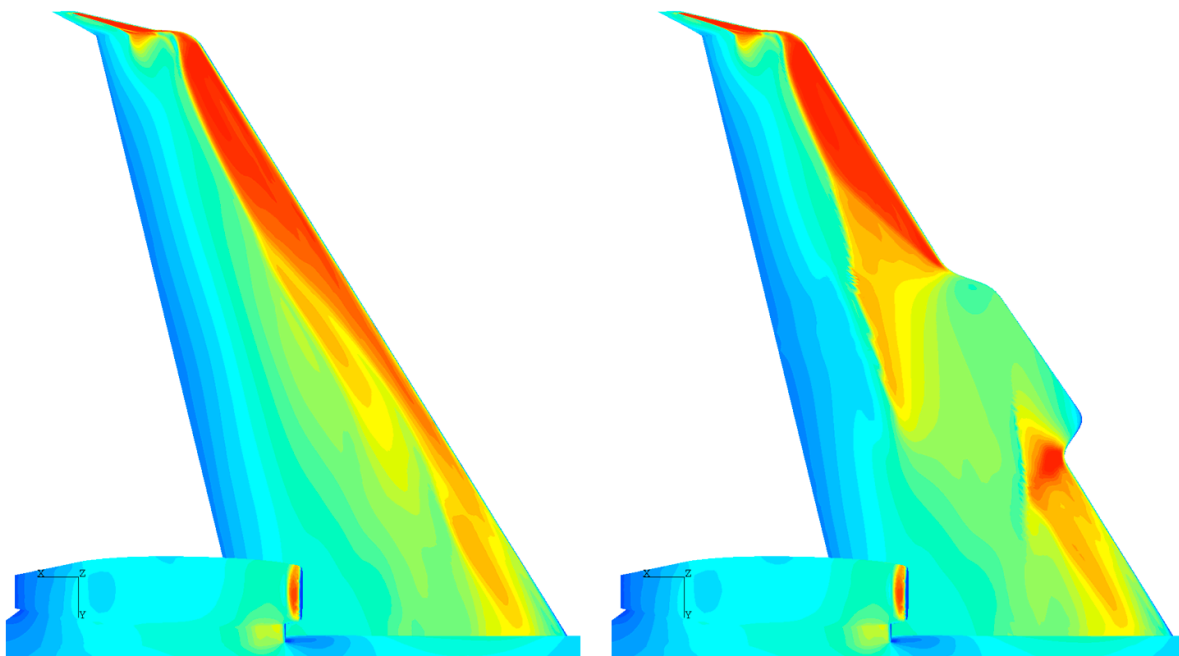


Figure 7. Upper surface Mach contours of the clean and gloved wing at flight condition 2, and alpha 4.24° .

The clean wing shows a weak transonic shock on the inboard portion of the wing that develops into a strong shock further outboard. The test section eliminates the supersonic pocket near the leading edge of the wing in the gloved region. Even though there is no supersonic flow near the leading edge, the flow accelerates and eventually produces a new strong shock on the upper surface near the wing glove-blending region (aft portion of the glove). The glove also produces a pocket of supersonic flow that terminates in a shock at the inboard fairing region of the wing glove. The glove introduces a 'kink' in the leading edge sweep of the wing, which causes the small pocket of supersonic flow. Even though the glove changes the shock structure on the wing, the change is not significant enough to have a large impact on the overall aerodynamics of the business jet. The effects of the span load lift force and pitching moment around the quarter chord are shown in Fig. 8.

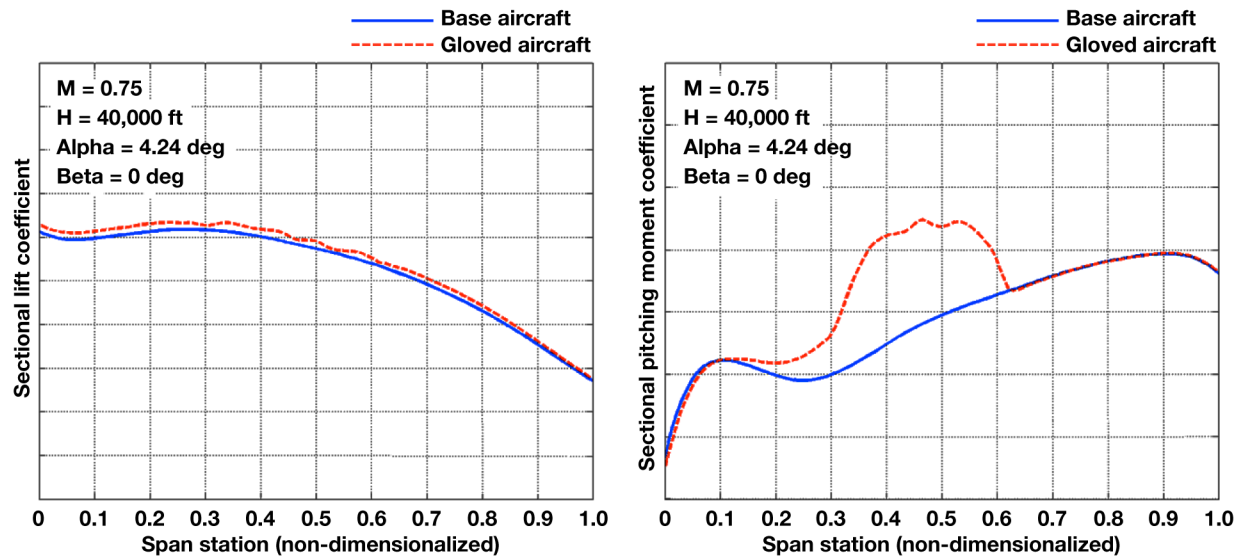


Figure 8. Flight condition 2; alpha 4.24°. Left: span lift coefficient on the left wing. Right: span pitching moment coefficient about the quarter-chord on the left wing.

The span-load plots presented are non-dimensionalized by the clean wing mean aerodynamic chord (MAC). This allows for a valid comparison between the coefficients of the wing and the glove, and shows the trend of the forces produced on the wing. The span lift distribution of the glove matches very nicely with the clean wing. This minimal change in lift is the reason why the rolling moment of the aircraft does not change significantly with the addition of the glove. The minimal change in lift distribution signifies that there will be a minimal change in the wing root bending moment of the aircraft. The change in pitching moment about the quarter-chord is to be expected with the glove since the lift is distributed differently over the larger chord sections. This extension causes a much larger torsional moment about the quarter-chord at this flight condition, and consequently, a pitch up moment for the entire aircraft. Adding sideslip to the aircraft in either direction does not change the span loading significantly.

Flight conditions one and three showed no more unexpected flow phenomena and showed all of the same trends as flight condition two. However, flight condition four at M_∞ 0.85, and H 25,000 ft, showed very different trends and phenomena than any of the other flight conditions. The upper surface Mach contours at an aircraft alpha of 1.59° are shown in Fig. 9.

There is a large difference in the location and magnitude of the shocks on the upper surface of the wing. Without the glove, there are prominent shocks along the entire span of the wing. The engine affects the flow over the wing inboard of the 50% span location. The biggest change in the flow over the wing, caused by the glove, is the addition of the shock around 50% span. Mach contours of a 2D slice of the center span location of the glove are shown in Fig. 10. The flow accelerates over the upper surface of the glove to supercritical speeds as it reaches the concave blending region. The flow then forms an expansion wave causing it to accelerate over the blending region. As the flow begins to compress when it reaches the baseline wing section, it slows back down and eventually terminates in a very strong shock on the aft portion of the wing. Even though this shock is stronger and further aft on the glove than the one on the clean wing, the average Mach over the entire upper surface is lower with the glove attached. The flow over the clean wing reaches supercriticality sooner and over a larger chord than that on the gloved wing. Since the lower surface flow is not changed very significantly, the gloved wing has less lift than the clean aircraft wing, as seen in Fig. 11. The glove also influences the wing outboard of the glove. The shocks on the outboard portion of the wing with the glove terminate slightly farther forward than on the clean wing. Because the shock terminates sooner, the lift on the outboard portion of the wing decreases as well, which causes the aircraft to roll and yaw into the gloved wing. This is opposite of the trends for almost every other flight condition that has been analyzed.

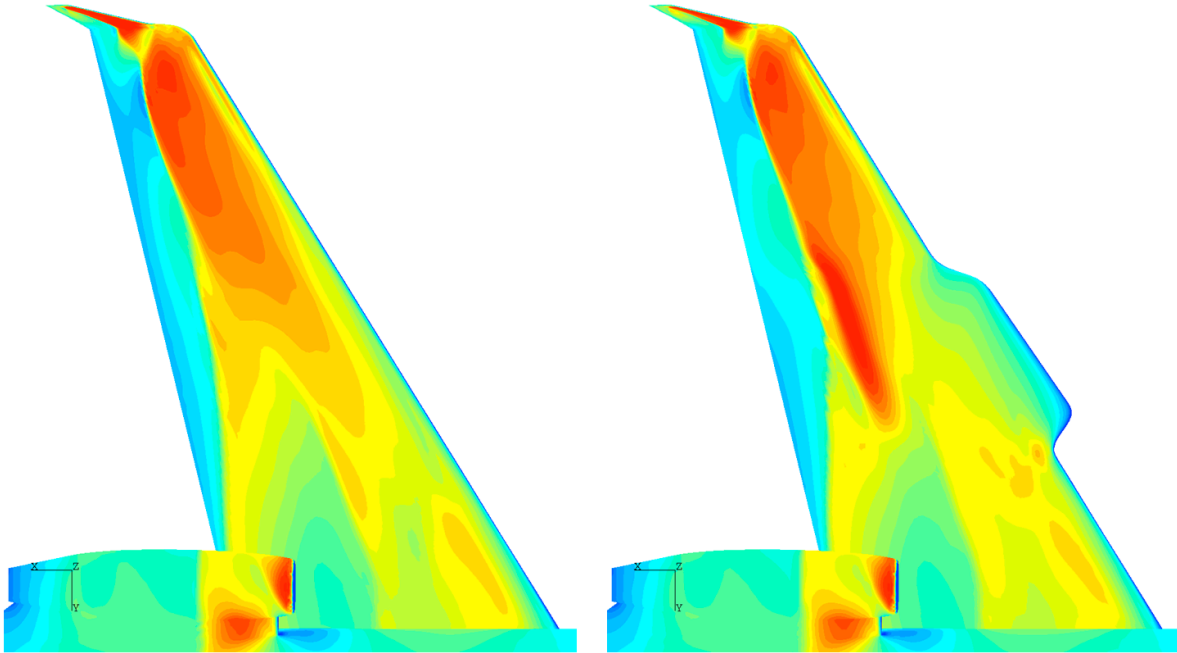


Figure 9. Upper surface Mach contours of the clean and gloved wing at flight condition 4, and alpha 1.59°.

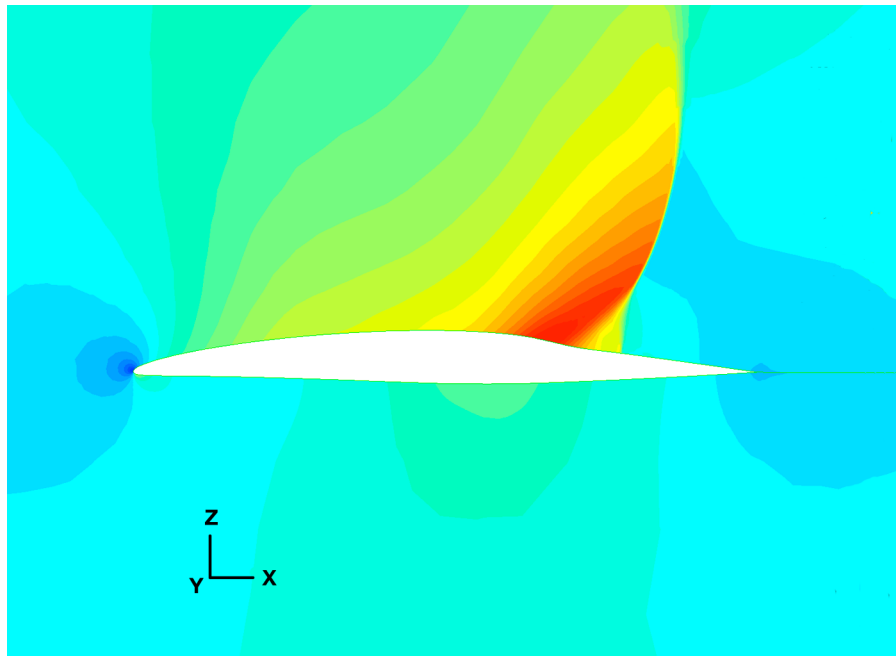


Figure 10. Mach contours center span of the glove at flight condition 4, and alpha 1.59°.

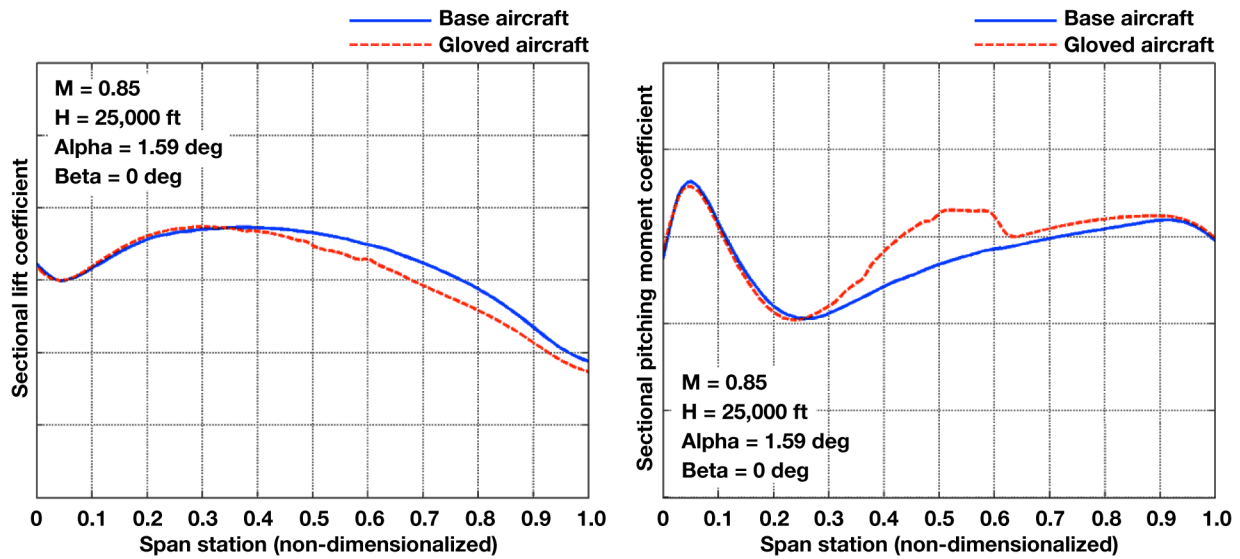


Figure 11. Flight condition 4; alpha 1.59°. Left: span lift coefficient on the left wing. Right: span pitching moment coefficient about the quarter-chord on the left wing.

Figure 11 shows, that the glove decreases the lift on the left wing. However, the torsional moment about the quarter-chord is increased slightly because the leading edge section of the glove protrudes forward from the clean wing. When the alpha is decreased by 1°, at the same flight condition, the effects of the glove change significantly. At 0.59°, the glove causes the aircraft to pitch down (opposite of trends), roll into the right wing (follows the trends), and yaw into the left wing (opposite of trends). There are no plans to fly out to maximum dynamic pressure, but even so, the control deflections required to trim the aircraft are still small. Figure 12 displays the span loading of the lift and pitching moment coefficients.

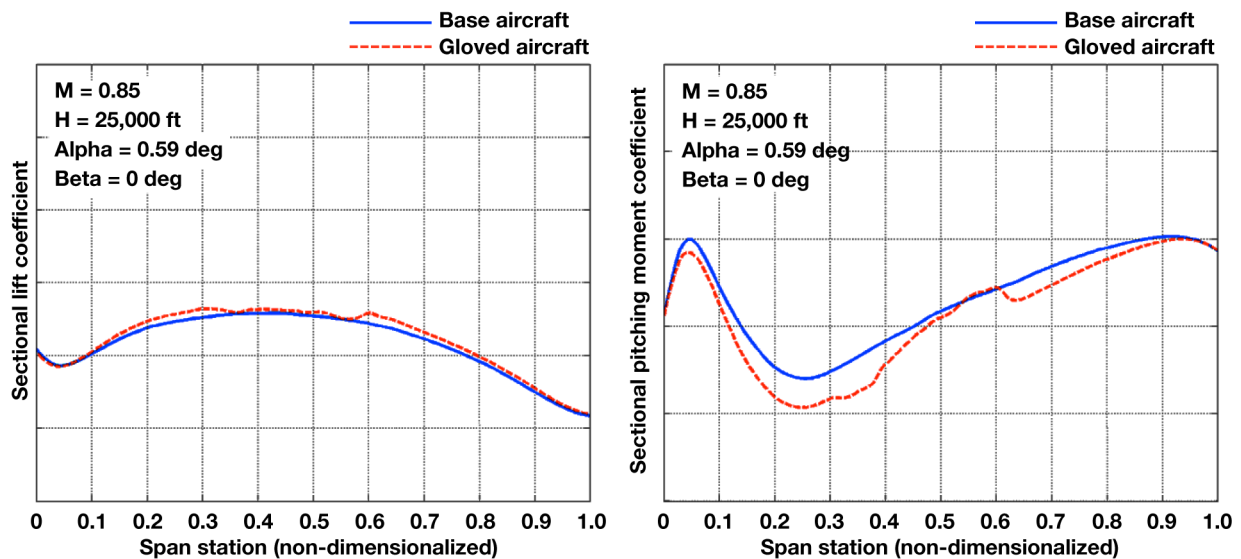


Figure 12. Flight condition 4; alpha 0.59°. Left: span lift coefficient on the left wing. Right: span pitching moment coefficient about the quarter-chord on the left wing.

At this alpha, the glove decreases the local lift in the gloved region, but slightly increases the lift on the rest of the wing. Locally, the lift does not increase in the glove region because there is an added pocket of negative lift at the leading edge of the glove that works to offset the slight increase in lift caused by the strong shock on the aft

portion of the glove. The chord-wise distribution of this lift is different, however, and causes a pitch-down moment around the quarter-chord. This in turn results in an added pitch down moment for the aircraft when the glove is attached. Because the lift increases slightly on the gloved wing, the aircraft will roll into the right wing. The added shock aft of the glove also results in a large increase in drag. At the low alpha configuration, the added drag outweighs the lift contribution in the axial direction, which is enough to cause the aircraft to yaw slightly into the left wing. The surface deflections required to trim out these moments is still well within the control limits of the aircraft as shown in Section IV.A.

The low speed results without the flaps deployed show benign flow characteristics because the aircraft is flying well away from the transonic regime. At an alpha of 10.67° , the span load lift coefficient does not change significantly. However, Fig. 13 shows that the pitching moment about the quarter-chord varies greatly between the gloved and clean wings.

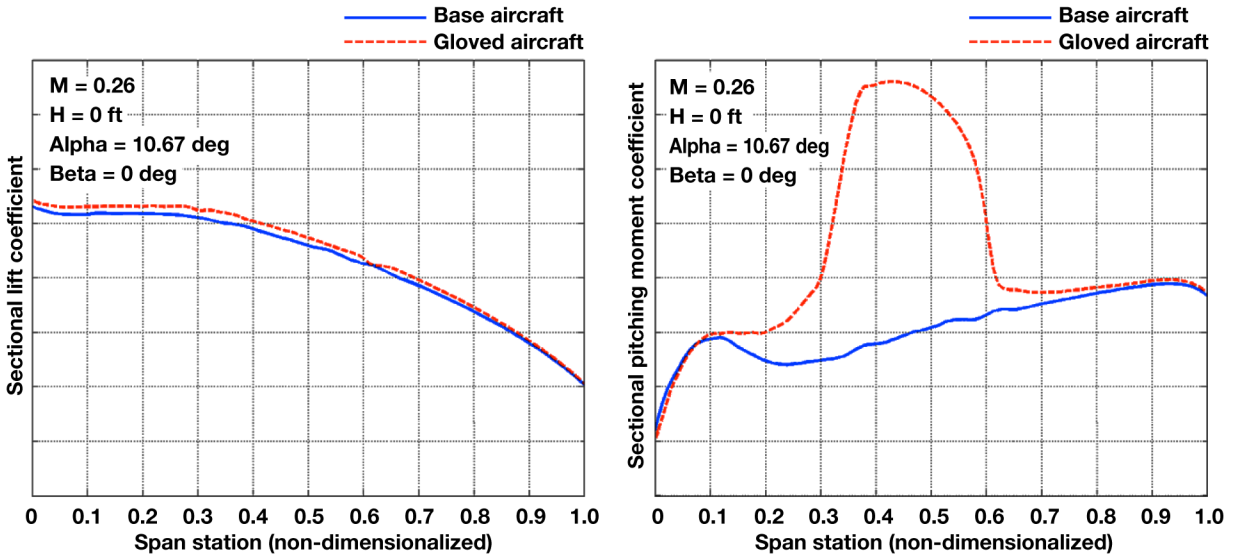


Figure 13. Flight condition 5, alpha 10.67° . Left: span lift coefficient on the left wing. Right: span pitching moment coefficient about the quarter-chord on the left wing.

There is a very large change in pitching moment because of the extension of the glove from the wing leading edge. The change in pitching moment is greatest at this flight condition and alpha, and could potentially present structural problems if the wing structure is not designed to sustain these types of loads.

Lastly, the aerodynamic effects of the glove on the aircraft are analyzed at a severe flight condition. The aircraft has just taken off and reaches V_2 , with flaps deployed, with one engine inoperable, and the aircraft is already yawing up to 15° into the dead engine. Even though this is a severe flight condition to be in, the results in Table 5 confirm that there are no added problems caused by the glove interacting with the flap, or the dead engine. Figure 14 shows pressure contours and streamlines coming off the aircraft at $M_\infty 0.22$, H 100 ft, 20° flaps, 6.75° alpha, and -15° beta, with OEI.

The streamlines of the flow traveling over the surface of the wings show that the glove does not produce any disruption in the flow. The glove does not affect the flow off of the flaps because the fowler flap has most of its flow coming from the pressure side of the wing. Similar results are seen at positive 15° of beta.

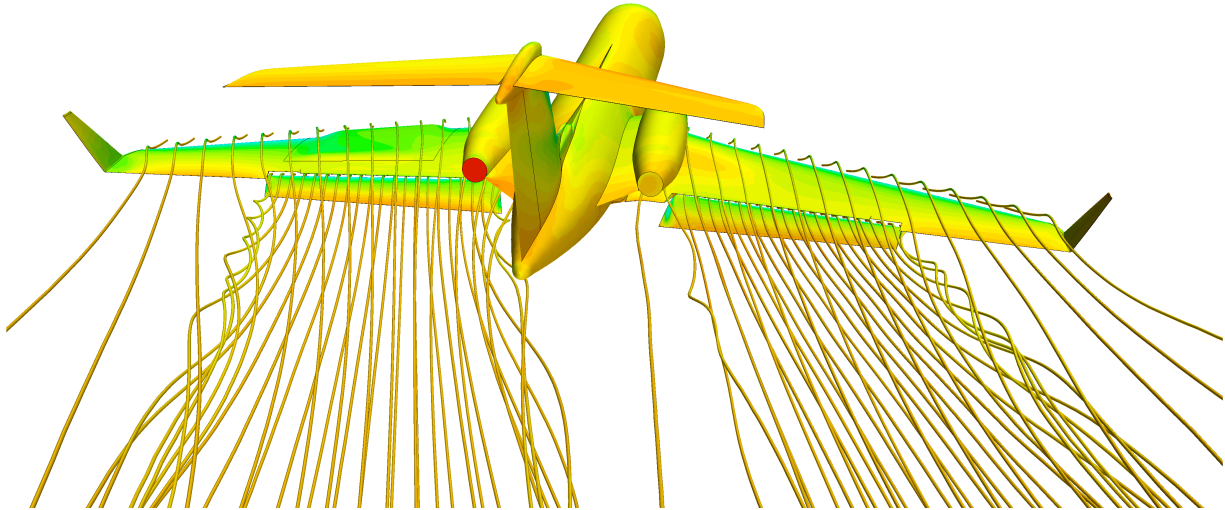


Figure 14. Pressure contours and streamlines at flight condition 7, alpha 6.75°, and beta -15°.

V. Conclusions

The delta aerodynamic forces and moments produced by the glove are fairly small, requiring only small control surface deflections to trim out the asymmetries produced by the glove. Overall, the glove has little effect on the aircraft aerodynamics at all of the flight conditions considered. The current glove increases overall lift and drag at most flight conditions. The added lift and drag cause the aircraft to roll to the right and yaw to the right because of roll/yaw coupling. The glove also produces a nose up pitching moment because of the protrusion from the leading edge of the wing. The lift distribution trend on the glove matches very nicely with that of the clean wing. The glove does add a large torsional load about the quarter-chord, which could be damaging to the wing structure. The glove does not produce any significant changes in the flow phenomena on the aircraft. At very high Mach number and dynamic pressure conditions, however, non-linear effects predominate and some reversal in the trends are seen.

TRANAIR and Star-CCM+ both worked very well in generating the necessary results for these studies. TRANAIR is a very accurate, fast turn-around program if the grid parameters are set correctly, and the flow conditions are within the applicability of the code. Star-CCM+ is very good for analyzing complex flows that TRANAIR cannot handle, and tends to be very robust in the grid generation and the solution accuracy.

The analysis in the paper is in support of a flight research experiment at NASA Dryden, therefore, flight data will be gathered that will include aircraft PID parameters, wing pressure distributions, surface temperatures, and much more. The CFD analysis will be compared against the flight data when it becomes available to help validate the current CFD analysis approach and identify areas where the computational analysis fails to accurately predict the in-flight flow phenomena.

References

1. TRANAIR, Software Package, Ver. 100, The Boeing Company, Chicago, Illinois, 2009.
2. AGPS, Aero Grid and Paneling System, Software Package, Ver. 22.12, Calmar Research Corporation, Cato, New York, 2007.
3. Star-CCM+, Software Package, Ver. 5.06.010, CD-adapco, Melville, New York, 2010.
4. Tinoco, E. N., "An Assessment of CFD Prediction of Drag and Other Longitudinal Characteristics," AIAA-2001-1002, *Proceedings of the 39th AIAA Aerospace Sciences Meeting & Exhibit*, Reno, Nevada, 8-11 January 2001.
5. TRANAIR User's Manual, Version 100, The Boeing Company, 2009.
6. Johnson, F. T., Tinoco, E. N., and Yu, N. J., "Thirty Years of Development and Application of CFD at Boeing Commercial Airplane, Seattle," AIAA-2003-3439, *Proceedings of the 16th AIAA Computational Fluid Dynamics Conference*, Orlando, Florida, 23-26 June, 2003.
7. Johnson, F. T., Samant, S. S., Bieterman, M. B., Melvin, R. G., Young, D. P., Bussoletti, J. E. and Hilmes, C. L., "TranAir: A Full-Potential, Solution-Adaptive, Rectangular Grid Code for Predicting Subsonic, Transonic, and Supersonic Flows About Arbitrary Configurations-Theory Document," NASA CR-4348, December 1992.
8. STAR-CCM+ User Guide, Version 6.02.008, CD-adapco, 2011.
9. Tinoco, E. N., "Validation and Minimizing CFD Uncertainty for Commercial Aircraft Applications," AIAA-2008-6902, *Proceedings of the 26th AIAA Applied Aerodynamics Conference*, Honolulu, Hawaii, 18-21, August 2008.

10. 3rd AIAA CFD Drag Prediction Workshop, San Francisco, California, 3-4 June 2006, URL: <http://aaac.larc.nasa.gov/tsab/cfdlarc/aiaa-dpw/Workshop3/> [cited 13 June, 2011].
11. NEPP, NASA Engine Performance Program, Software Package, NASA Glenn, Cleveland, OH, 1994.
12. Menter, F. R., "Zonal Two Equation $k-\omega$ Turbulence Models for Aerodynamic Flows," AIAA paper 93-2906, *Proceedings of the 24th Fluid Dynamics Conference*, Orlando, Florida, 6-9 July 1993.